2025 IEEE/SICE International Symposium on System Integration (SII)
January 21-24, 2025, Munich, Germany

# Wheel Gait Generation for Compass-like Biped Robot

Taiki Sedoguchi and Fumihiko Asano

*Abstract*— **This study discussed a generation of wheel gait for planar 4-DOF compass-like biped robot. Wheel gait is a novel locomotion pattern in which the stance leg swings in the opposite direction to that of a normal gait; that is, both the stance and swing legs rotate in the same direction. We derived dynamic equations of the robot and built an output tracking control of the hip angle. Next, we searched for fixed points using a numerical approach, and revealed that it is possible to generate a steady wheel gait on a slope with appropriate initial states. However, since the limit cycle around the fixed point was identicied to be unstable, it is expected that achieving a stable wheel gait with the control method in the real world is nearly impossible. On the other hand, small regions near the fixed point were found where stable period-2 gaits emerge, pointing to the possibility of stable wheel gait generation.**

## I. INTRODUCTION

As we walk forward, swinging our two legs alternately, the motion resembles two free pendulums oscillating in opposite phases. This is a physical analogy, as the swing leg is naturally swung out due to the gravitational effect. The relationship between walking and physical action is well illustrated by passive dynamic walking. Passive dynamic walking is a physical phenomenon in which a walking robot without actuators, given an appropriate initial state, walks down a slope solely by gravitational action. McGeer first studied passive dynamic walking and demonstrated generation of stable gaits without actuators, and the existence of limit cycles was proven [1]. Since then, a number of simple planar models of passive dynamic walker such as *"compass-like biped robot* [2]-[5]," *"three-link bipedal robot* [6]-[8]," *"five-link bipedal robot* [9]-[11]" and et al. have been proposed and studied with the motivation of elucidating the principles of human gait and generating a highly efficient gait.

On the other hand, wheel gait, in which the swing leg rotates in the opposite direction respect to the normal gait, is an unnatural gait and has been little studied as yet. One advantage of wheel gait is that it minimizes the risk of the swing leg scuffing against the ground. Kieffer et al. first proposed a wheel gait robot as a *"dynamically simple biped"* in 1993 [12]. The robot consists of two identical links and a reaction wheel, which are connected by a rotary drive joint at their center of mass. The primary advantage of this robot lies in the exceptional simplification of its equation of motion, achieved by keeping the center of gravity fixed at the robot's body center. The paper derives the equation of motion and collision as well as the step-to-step boundary conditions for periodic walking, and shows that the model can walk on both flat and inclined surfaces. Spong et al. also discussed the nonlinear control method of the robot using the linear approximation [13]. Asano et al. have refer to a class of robots with two identical frames connected at their center of mass via rotary drive joint as *"X-shaped walker,"* and have studied the generation of wheel gait, including analysis of models adding elements such as a reaction wheel or telescopic legs [14]-[16]. In addition, they have analyzed walking speed and efficiency and developed real robots inspired the X-shaped walker.

In this paper, we discuss the wheel gait generation for a compass-like biped robot. This is the first attempt to achieve a wheel gait in a well-known simplest bipedal model. It has already been demonstrated that the robot can walk passively on a slope without actuators, but is it possible to continue a stable walk applying the control input which rotates the swing leg in the opposite direction against the gravity force? This question is a mere academic interest, but could lead to expand the possibility of existing biped robots. For example, when there is a large obstacle in front of a robot, it may be able to overcome it easily if the robot can walk using wheel gait, which swings up the legs as well as a hurdle runner. This paper aims to clarify whether stable wheel gait generation is possible in the compass-like biped robot and to gain a deeper understanding about wheel gait.

## II. MODELING

### A. Equation of Motion

The model of the planar compass-like biped robot is shown in Fig. 1. The model consists of two identical leg frames with

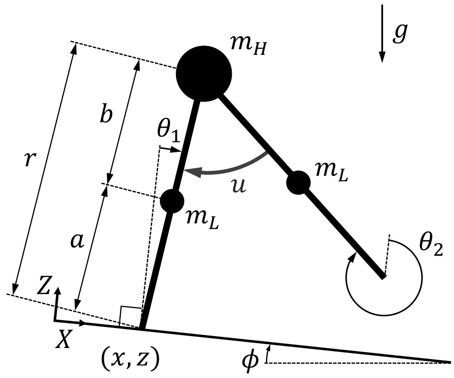


Fig. 1: Compass-like biped model.

*This work supported by Research and Development Grants for FY2024 from Azbil Yamatake General Foundation.

The authors are with the Graduate School of Advanced Science and Technology, Japan Advanced Institute of Science and Technology, 1-1 Asahidai Nomi, Ishikawa 923-1292, Japan {sedoguchi, fasano}@jaist.ac.jp

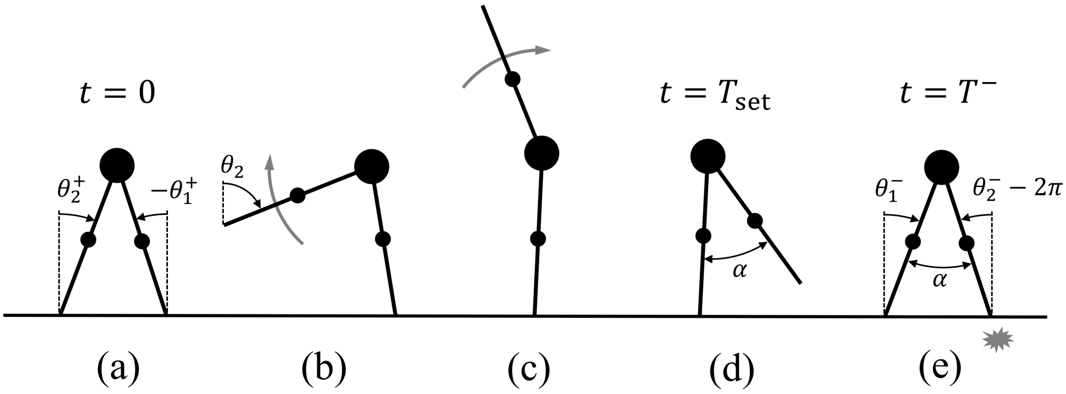


Fig. 2: Sequence diagram of wheel gait for one step.

three point masses, and this is identical to a double pendulum with one end fixed to the ground. The point masses at the hip joint and leg center are represented by $m_H$ and $m_L$, respectively. Let $a$ denote the distance between the leg mass and the leg tip, and $b$ the distance between the hip and the leg mass. The total leg length is expressed as $r := a + b$. The stance and swing leg angles relative to the ground are $\theta_1$ and $\theta_2$, respectively, with a rotational actuator at the hip joint controlling the hip angle. The angle between the slope and the horizontal direction is given by $\phi$. The horizontal and vertical directions relative to the slope are denoted as the $X$- and $Z$-directions, respectively, and the position of the swing leg tip is represented by the coordinates $(x, z)$. The equation of motion of the model is given as

$$\boldsymbol{M}\ddot{\boldsymbol{q}} + \boldsymbol{h} = \boldsymbol{S}u + \boldsymbol{J}_c^{\mathrm{T}}\boldsymbol{\lambda}_c, \tag{1}$$

where $\boldsymbol{q} = \left[\begin{array}{cccc} x & z & \theta_1 & \theta_2 \end{array}\right]^{\mathrm{T}}$ is the generalized coordinate vector, $\boldsymbol{M} \in \mathbb{R}^{4\times4}$ is the inertia matrix, $\boldsymbol{h} \in \mathbb{R}^4$ is the nonlinear force vector consists Coriolis forces, centrifugal forces and gravitational forces, $\boldsymbol{S} \in \mathbb{R}^4$ is the driving vector, $u$ is the control input, and $\boldsymbol{J}_c^{\mathrm{T}}\boldsymbol{\lambda}_c \in \mathbb{R}^4$ is the holonomic constraint force term. Details of the inertia matrix and the nonlinear force vector are given in the Appendix. The driving vector detailed as

$$\boldsymbol{S} = \left[\begin{array}{cccc} 0 & 0 & 1 & -1 \end{array}\right]^{\mathrm{T}}. \tag{2}$$

We assume that the tip of the stance leg is always in contact the ground without sliding, so the velocity constraint conditions are given as $\dot{x} = 0$ and $\dot{z} = 0$. These equations can be arranged to

$$\boldsymbol{J}_c\dot{\boldsymbol{q}} = \boldsymbol{0}_{2\times1}, \quad \boldsymbol{J}_c = \left[\begin{array}{ccccc} 1 & 0 & 0 & 0 & 0 \\ 0 & 1 & 0 & 0 & 0 \end{array}\right]. \tag{3}$$

$\boldsymbol{\lambda}_c \in \mathbb{R}^2$ is the ground reaction force vector consisting of the ground forces in the $X$ and $Z$-direction, $F_x$ and $F_z$, and it is obtained by summarizing Eqs. (1) and (2).

$$\begin{aligned} \boldsymbol{\lambda}_c &= -\boldsymbol{X}_c^{-1}\boldsymbol{J}_c\boldsymbol{M}^{-1}(\boldsymbol{S}u - \boldsymbol{h}) = \left[\begin{array}{c} F_x \\ F_z \end{array}\right] \\ \boldsymbol{X}_c &:= \boldsymbol{J}_c\boldsymbol{M}^{-1}\boldsymbol{J}_c^{\mathrm{T}} \end{aligned} \tag{4}$$

Then, from Eqs. (1) and (3), the acceleration vector can be derived as:

$$\ddot{\boldsymbol{q}} = \boldsymbol{M}^{-1}\boldsymbol{Y}_c\left(\boldsymbol{S}\boldsymbol{u} - \boldsymbol{h}\right), \tag{5}$$

where $\boldsymbol{Y}_c := \boldsymbol{I}_4 - \boldsymbol{J}_c^{\mathrm{T}}\boldsymbol{X}_c^{-1}\boldsymbol{J}_c\boldsymbol{M}^{-1}$, and $\boldsymbol{I}_4 \in \mathbb{R}^{4\times4}$ is an identity matrix.

### B. Equation of Collision

In this paper, we assume that the fore leg always collide with the ground without sliding, and the rear leg takes off immediately after the completely inelastic collision with the ground. The collision equation is given as

$$\boldsymbol{M}\dot{\boldsymbol{q}}^+ = \boldsymbol{M}\dot{\boldsymbol{q}}^- + \boldsymbol{J}_I^{\mathrm{T}}\boldsymbol{\lambda}_I. \tag{6}$$

Here the superscripts "$-$" and "$+$" shall denote immediately before and after impact, and $\boldsymbol{\lambda}_I \in \mathbb{R}^2$ represents the impulse vector determined as the zero-time integral of impulse force. The velocity constraint condition that should hold for the tip position of the swing leg immediately after landing becomes

$$\boldsymbol{J}_I\dot{\boldsymbol{q}}^+ = \boldsymbol{0}_{2\times1}, \tag{7}$$

where the detail of the Jacobian matrix $\boldsymbol{J}_I$ is

$$\boldsymbol{J}_I = \left[\begin{array}{cccc} 1 & 0 & r\cos\theta_1 & -r\cos\theta_2 \\ 0 & 1 & -r\sin\theta_1 & r\sin\theta_2 \end{array}\right]. \tag{8}$$

Following Eqs. (10) and (11), the velocity vector immediately after impact is given as

$$\dot{\boldsymbol{q}}^+ = \left(\boldsymbol{I}_4 - \boldsymbol{M}^{-1}\boldsymbol{J}_I^{\mathrm{T}}\left(\boldsymbol{J}_I\boldsymbol{M}^{-1}\boldsymbol{J}_I^{\mathrm{T}}\right)^{-1}\boldsymbol{J}_I\right)\dot{\boldsymbol{q}}^-. \tag{9}$$

Finally, the update of the position and velocity coordinates are completed by resetting each component of $\boldsymbol{q}^+$ and $\dot{\boldsymbol{q}}^+$, taking into account the stance leg exchange.

$$\left[\begin{array}{c} x^+ \\ z^+ \\ \theta_1^+ \\ \theta_2^+ \end{array}\right] = \left[\begin{array}{c} x^- + r\sin\theta_1^- + r\sin\theta_2^- \\ 0 \\ \theta_2^- - 2\pi \\ \theta_1^- \end{array}\right] \tag{10}$$

$$\left[\begin{array}{c} \dot{x}^+ \\ \dot{z}^+ \\ \dot{\theta}_1^+ \\ \dot{\theta}_2^+ \end{array}\right] = \left[\begin{array}{cccc} 0 & 0 & 0 & 0 \\ 0 & 0 & 0 & 0 \\ 0 & 0 & 0 & 1 \\ 0 & 0 & 1 & 0 \end{array}\right]\dot{\boldsymbol{q}}^+ \tag{11}$$

In Eq. (10), $\theta_1^+ = -\theta_2^+ = -\alpha/2$ holds where $\alpha \in [0, \pi]$ [rad] is the "smaller" relative hip-joint angle at impact. Also, it should be noted that $2\pi$ is subtracted from the angular position of the swing leg in the third row to reset the absolute angle; this operation is not necessary in the modeling of the normal gait.

## III. CONTROL METHOD

### A. Input-output Linearization

In this paper, we build the output tracking control of the relative hip-joint angle shown in Fig. 2, as one of simple nonlinear control methods. Define the control output as

$$y := \boldsymbol{S}^{\mathrm{T}} \boldsymbol{q} = \theta_1 - \theta_2. \tag{12}$$

The second-order derivative with respect to time is then

$$\ddot{y} = \boldsymbol{S}^{\mathrm{T}} \ddot{\boldsymbol{q}} = \boldsymbol{S}^{\mathrm{T}} \boldsymbol{M}^{-1} \boldsymbol{Y}_c \left( \boldsymbol{S} u - \boldsymbol{h} \right). \tag{13}$$

Define the desired control output as $y_{\mathrm{d}}(t)$, where $t$ is a time variable which is reset to zero following each collision. Then, we can determine the control input for achieving $y \to y_{\mathrm{d}}(t)$ as

$$u = \left( \boldsymbol{S}^{\mathrm{T}} \boldsymbol{M}^{-1} \boldsymbol{Y}_c \boldsymbol{S} \right)^{-1} \left( v + \boldsymbol{S}^{\mathrm{T}} \boldsymbol{M}^{-1} \boldsymbol{Y}_c \boldsymbol{h} \right), \tag{14}$$

$$v = \ddot{y}_{\mathrm{d}}(t) + k_d \left( \dot{y}_{\mathrm{d}}(t) - \dot{y} \right) + k_p \left( y_{\mathrm{d}}(t) - y \right), \tag{15}$$

where $k_d > 0$ and $k_p > 0$ are the derivative gain constant and the proportional gain constant, respectively. Also, $v \in \mathbb{R}$ is the desired acceleration command signal.

### B. Design of Desired Time Trajectory

We design a desired time trajectory from initial and terminal states of the control output values. Define $T$ be the step period, $T_{\mathrm{set}}$ be the desired settling time of $y$, and $y_{\mathrm{set}} = \alpha - 2\pi$ be the desired terminal value of the output. In order to avoid heavy variations of the control input and to achieve smooth leg rotations, the boundary conditions of the desired trajectory are set as follows:

$$y_{\mathrm{d}}(0) = y^+, \ \dot{y}_{\mathrm{d}}(0) = \dot{y}^+, \ \ddot{y}_{\mathrm{d}}(0) = 0,$$
$$y_{\mathrm{d}}(T_{\mathrm{set}}) = y_{\mathrm{set}}, \ \dot{y}_{\mathrm{d}}(T_{\mathrm{set}}) = 0, \ \ddot{y}_{\mathrm{d}}(T_{\mathrm{set}}) = 0.$$

The desired trajectory to achieve the boundary conditions can be represented by the following 5-order time-dependent function.

$$y_{\mathrm{d}}(t) = \begin{cases} \sum_{k=0}^{n} a_k t^k & (0 \le t < T_{\mathrm{set}}) \\ y_{\mathrm{set}} & (T_{\mathrm{set}} \le t < T) \end{cases} \tag{16}$$

The coefficients $a_k \in \mathbb{R}$ in the function are given as follows.

$$\begin{bmatrix} a_5 \\ a_4 \\ a_3 \\ a_2 \\ a_1 \\ a_0 \end{bmatrix} = \begin{bmatrix} -3\left(\dot{y}^+ T_{\mathrm{set}} + 2y^+ - 2y_{\mathrm{set}}\right)/T_{\mathrm{set}}^5 \\ \left(8\dot{y}^+ T_{\mathrm{set}} + 15y^+ - 15y_{\mathrm{set}}\right)/T_{\mathrm{set}}^4 \\ -2\left(3\dot{y}^+ T_{\mathrm{set}} + 5y^+ - 5y_{\mathrm{set}}\right)/T_{\mathrm{set}}^3 \\ 0 \\ \dot{y}^+ \\ y^+ \end{bmatrix} \tag{17}$$

## IV. SEARCHING FOR FIXED POINT

### A. Fixed Point

In the biped robot field, fixed point means the point on the limit cycle where $\boldsymbol{x}^{(k+1)} = \boldsymbol{f}(\boldsymbol{x}^{(k)}) = \boldsymbol{x}^{(k)}$ [17]. Here, $\boldsymbol{x}^{(k)}$ refers to a discrete state variable vector immediately after the impact of $k$-th step, and $\boldsymbol{f}(\boldsymbol{x}^{(k)})$ is a Poincaré map of $\boldsymbol{x}^{(k)}$. Let $\boldsymbol{x}^*$ denote a fixed point satisfying $\boldsymbol{f}(\boldsymbol{x}^*) = \boldsymbol{x}^*$. If there are no disturbances or terrain changes and the state is at the fixed point, the gait becomes steady. Whereas a gait on the above limit cycle is called *"period-1 gait,"* a gait that returns to the same state every *two* steps is called "*period-2 gait*." A period-2 gait can be expressed as $\boldsymbol{x}^{(k+2)} = \boldsymbol{f}(\boldsymbol{f}(\boldsymbol{x}^{(k)})) = \boldsymbol{x}^{(k)}$, in addition, three or even more multi-period gait can be denoted in the similar format.

If the limit cycle is stable, the state is attracted back to a steady state again even if the state slightly deviates from the fixed point [2]. The stability of a fixed point can be evaluated by analyzing the eigenvalues of the Jacobian matrix $\boldsymbol{J}$ [18]. A small perturbation of the state vector from a fixed point at $k$-th step, $\Delta\boldsymbol{x}^{(k)}$, will be amplified or reduced step-by-step approximately according to

$$\Delta\boldsymbol{x}^{(k+1)} \approx \boldsymbol{J}\Delta\boldsymbol{x}^{(k)}, \ \ \boldsymbol{J} := \left.\frac{\partial \boldsymbol{f}}{\partial \boldsymbol{x}}\right|_{\boldsymbol{x}=\boldsymbol{x}^*}. \tag{18}$$

If all of the eigenvalues of $\boldsymbol{J}$ are located within the unit circle on the complex plane, the perturbation will decay to $\boldsymbol{0}$, i.e. the limit cycle is stable at the fixed point. Conversely, the eigenvalues outside the unit circle make the system unstable and collapse the limit cycle with a micro perturbation.

In the model of this paper, if the output tracking control has been completed without lifting the stance leg, it is sufficient to consider the stability of the angular velocity of the stance leg, $\dot{\theta}_1$, and there is no need to take other state variables into account. The difference equation for the perturbation in the angular velocity from a fixed point, $\Delta\dot{\theta}_1^{(k)}$, is obtained as follows:

$$\Delta\dot{\theta}_1^{(k+1)} \approx J_{\dot{\theta}_1} \Delta\dot{\theta}_1^{(k)}, \quad J_{\dot{\theta}_1} := \frac{\partial \dot{\theta}_1^{(k+1)}}{\partial \dot{\theta}_1^{(k)}}. \tag{19}$$

It can be concluded that the gait is stable under $||J_{\dot{\theta}_1}|| < 1$. However, it is difficult to determine the value theoretically because of its complexity; therefore, numerical approaches are commonly used.

### B. Simulation Result

In this section, we conduct an exhaustive search with respect to the parameters $\phi$, $\alpha$, $T_{\mathrm{set}}$ and $\dot{\theta}_1^{(1)}$. To simplify the setting of initial values, the initial state is set as the state immediately before impact after the control has been completed. The values of the initial state are as follows:

$$q(0) = \begin{bmatrix} 0 \\ 0 \\ \alpha/2 \\ 2\pi - \alpha/2 \end{bmatrix}, \ \dot{q}(0) = \begin{bmatrix} 0 \\ 0 \\ \dot{\theta}^- \\ \dot{\theta}^- \end{bmatrix}, \tag{20}$$

where $\dot{\theta}^-$ is the angular velocity of the legs immediately before collision. The physical and control parameters for the simulation are listed in Table I.

TABLE I: Physical and control parameters.

| | | | | | |
|---|---|---|---|---|---|
| $m_H$ | 1.0 | kg | $g$ | 9.81 | m/s$^2$ |
| $m_L$ | 0.5 | kg | $k_d$ | 100 | s$^{-1}$ |
| $a$ | 0.5 | m | $k_p$ | 2500 | s$^{-2}$ |
| $b$ | 0.5 | m | | | |

Fig. 3 displays the analysis results of the fixed-point search. Three conditions must be satisfied: (i) the swing leg must remain in contact with the ground ($F_z > 0$); (ii) the angular positions immediately after impact must satisfy the required values ($\theta_1^+ = -\theta_2^+ = -\alpha/2$); and (iii) the control process must be completed ($T_{\text{set}} \leq T$). Steps that failed to meet these conditions were considered failures and excluded from the results.

The figure shows the difference in the angular velocity of the swing leg immediately after collision between first and second steps, $\dot{\theta}_1^{(2)} - \dot{\theta}_1^{(1)}$, with respect to $\dot{\theta}_1^{(1)}$ and $T_{\text{set}}$. When the angular velocity difference between the two steps becomes zero and hip angle control has been completed (as highlighted in red in the figures), that is, when the angular position and velocity between steps remain unchanged, a steady gait can be generated. Fig. 3 (a) illustrates the existence of fixed points where $\phi = 0.05$ [rad] and within in the range $0.40 \leq \alpha \leq 0.55$ [rad]. Similarly, Fig. 3 (b) shows fixed points where $\phi = 0.07$ [rad] and $0.50 \leq \alpha \leq 0.60$ [rad]. It can be seen that as $\alpha$ increases, the walkable area shifts to regions where $\dot{\theta}_1^{(1)}$ is larger. On the other hand, the conditions were not met, and the walking failed in most areas. The primary cause of these failures was the negative ground force in the $Z$-direction of the stance leg during the deceleration phase of the swing leg, highlighting the difficulty of achieving a wheel gait.

An example of the relationship between $\dot{\theta}^{(2)}$ and $T_{\text{set}}$ is shown in Fig. 4. In the area where $T_{\text{set}}$ is small ($T_{\text{set}} < 0.99$ [s]), i.e. the control of the hip angle is controlled rapidly, the robot could not overcome the potential barrier due to the large counter-torque caused by the fast rotational acceleration of the swing leg. Furthermore, the rapid deceleration after acceleration is accompanied by an increase in the upward force generated, which in turn facilitates the take-off of the robot. Conversely, if $T_{\text{set}}$ is too large ($T_{\text{set}} \geq 1.18$ [s]), the tip of the swing leg contacts with the ground before the completion of control of the swing leg. Of course, $\dot{\theta}_1^{(1)}$ is also related to the feasibility of walking; if $\dot{\theta}_1^{(1)}$ is lower than the appropriate value, the robot cannot overcome the potential barrier, and conversely, if it is excessive, the control cannot be completed. These results suggest that the region in which fixed points can be found is extremely limited due to the various constraints.

## V. GAIT ANALYSIS

### A. Typical Wheel Gait

From the previous chapter, it can be observed that there are fixed points which achieve steady gaits with appropriate initial states. In this chapter, we used Newton's method to determine a fixed point, followed by a detailed analysis. The parameters corresponding to the fixed point are listed

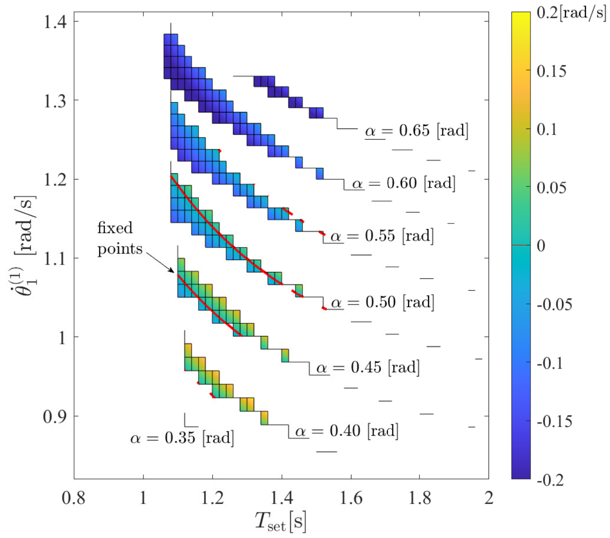


(a) $\phi = 0.05$ [rad]

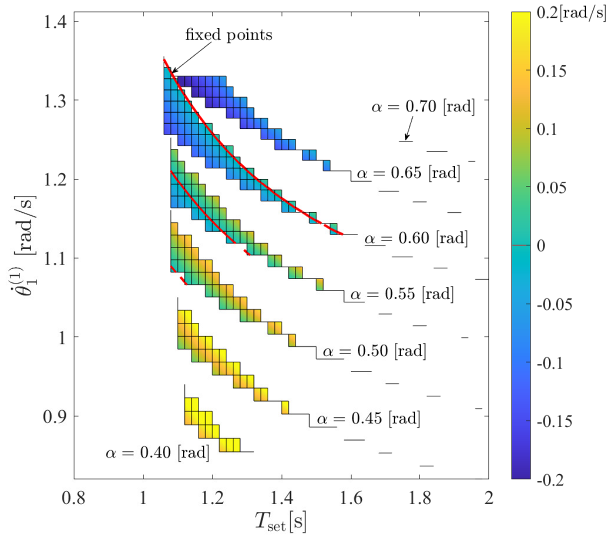


(b) $\phi = 0.07$ [rad]

Fig. 3: Differences in angular velocity of swing leg immediately after collision between first and second steps, $\dot{\theta}_1^{(2)} - \dot{\theta}_1^{(1)}$.

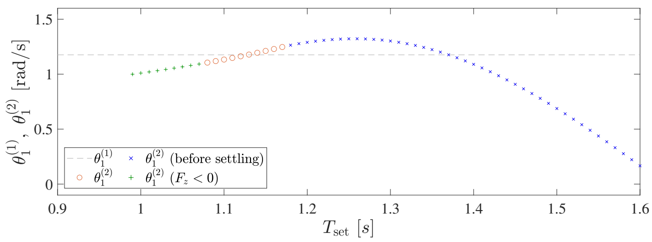


Fig. 4: Angular velocity of swing leg immediately after impact at second step, $\dot{\theta}_1^{(2)}$, respect to $T_{\text{set}}$ where $\phi = 0.05$ [rad], $\alpha = 0.5$ [rad], $\dot{\theta}^- = 1.5$ [rad/s] and $\dot{\theta}_1^{(1)} = 1.175852$ [rad/s].

TABLE II: Parameters for typical wheel gait.

| | | |
|---|---|---|
| $\phi$ | 0.05 | rad |
| $T_{\text{set}}$ | 1.12842 | s |
| $\dot{\theta}^{-}$ | 1.5 | rad/s |
| $\alpha$ | 0.5 | rad |

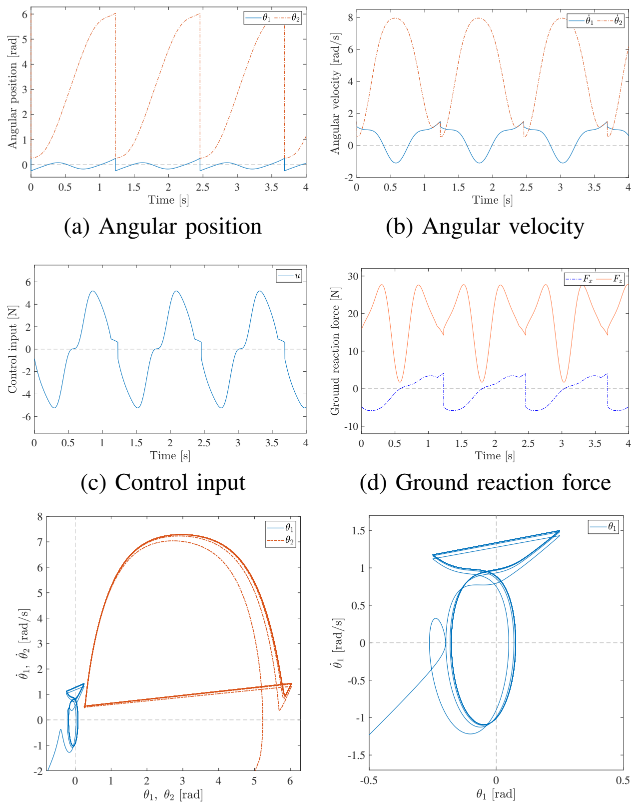


(a) Angular position (b) Angular velocity

(c) Control input (d) Ground reaction force

(e) Phase diagram for $\theta_1$ and $\theta_2$ (f) Phase diagram for $\theta_1$

Fig. 5: Simulation results of typical wheel gait.

in Table II, while the other parameters are identical to those in Table I. Fig. 5 shows the simulation results of the typical wheel gait generation. In the Fig. 5, (a) is the angular positions of the legs, $\theta_1$ and $\theta_2$, (b) is the angular velocities, $\dot{\theta}_1$ and $\dot{\theta}_2$, (c) is the control input, $u$, (d) is the ground reaction forces, $F_x$ and $F_z$, (e) and (f) are phase diagrams. Moreover, the stick diagram at the first step of the typical wheel gait is shown in Fig. 6.

At first glance, the simulation results appear to indicate the generation of a periodic wheel gait, however, Fig. 5 (e) and (f) show that the gait is not steady. The walking failed at step 11 because the potential barrier could not be overcome. Although the parameters in Table II are set as close as possible to the fixed point, a micro error still exists. As mentioned above, if the limit cycle is stable, the state would return to the fixed point, however, the attraction was not observed. Numerical partial differentiation using the central difference method with a step width of $1 \times 10^{-5}$ [rad/s] at the fixed point yields $J_{\dot{\theta}_1}$ in Eq. (19) of 1.43484, indicating instability of the gait. As shown in Figure 6, the stance leg initially rotates forward immediately after impact. However, it subsequently reverses direction as a result of the counter-torque induced by the swing leg's rotation.

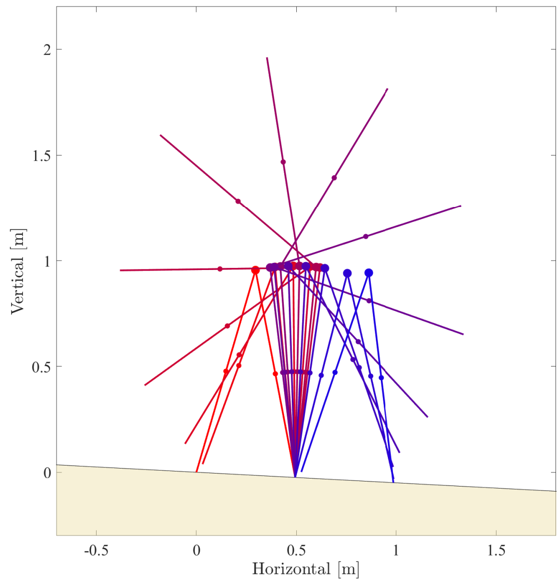


Fig. 6: Stick diagram of typical wheel gait.

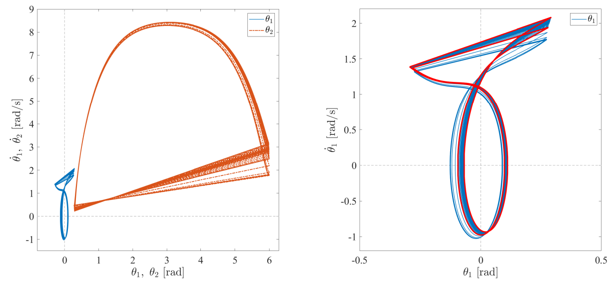

(a) Phase diagram for $\theta_1$ and $\theta_2$ (b) Phase diagram for $\theta_1$

Fig. 7: Phase diagram of stable period-2 gait where $\phi = 0.05$ [rad], $\alpha = 0.55$ [rad], $T_{\text{set}} = 1.08752$ [s] and $\dot{\theta}^{-} = 1.76674$ [rad/s].

### B. *Stable Period-2 Gait*

Fig. 7 shows a stable period-2 wheel gait discovered unexpectedly. The figure illustrates that the unstable period-1 gait starting from an immediate vicinity of a fixed point converges to a period-2 gait. In Fig. 7 (b), the period-2 gait is highlighted in red. A notable feature is that the swing leg makes ground contact before the control is completed, a case classified as a failure in the previous simulations. The bifurcation and chaos phenomenon of walking has been observed in a region close to limit point of gait stability [2][3], indicating that a stable region of wheel gait even for the compass-liked robot may appear by changing the control method and physical parameters. Detailed stability analysis needs to be carried out in the future.

## VI. CONCLUSIONS

In this paper, we achieved the wheel gait generation for planar 4-DOF compass-liked biped robot on a slope using the output tracking control for the target time trajectory. Nevertheless, it was observed that the generation of stable wheel gait is very difficult due to the instability of limit cycle. The angle of a slope, the target hip angle, the target settling time and the initial angular velocities of the legs are intricately related to gait stability, and even the slightest error from the fixed point will cause gait to fail. On the other hand, we identified a period-2 gait pattern, which suggests the potential for generating a stable wheel gait.

The relationship between gait stability and gait stabilization through improved control methods should be studied in detail in the future. The generation of a wheel gait on a horizontal plane and uneven terrain by adding actuators is also considered a promising approach.

## APPENDIX

### A. Details of Inertia Matrix and Nonlinear Force Vector

The inertia matrix $\boldsymbol{M}$, and nonlinear force vector $\boldsymbol{h}$ are given as follows.

$$\boldsymbol{M} = \begin{bmatrix} m & 0 & M_{13} & M_{14} \\ & m & M_{23} & M_{24} \\ & & m_1 r^2 + m_L a^2 & M_{34} \\ \text{Sym.} & & & m_L b^2 \end{bmatrix}$$

$$\begin{aligned}
m &= m_H + 2m_L \\
m_1 &= m_H + m_L \\
m_2 &= m_1 r + m_L a \\
M_{13} &= m_2 \cos\theta_1 \\
M_{14} &= -m_L b \cos\theta_2 \\
M_{23} &= -(m_1 r + m_L a)\sin\theta_1 \\
M_{24} &= m_L b \sin\theta_2 \\
M_{34} &= -m_L r b \cos(\theta_1 - \theta_2) \\
\boldsymbol{h} &= \begin{bmatrix} -mg\sin\phi - m_2\dot{\theta}_1^2 \sin\theta_1 + m_L b\dot{\theta}_2^2 \sin\theta_2 \\ mg\cos\phi - m_2\dot{\theta}_1^2\cos\theta_1 + m_L b\dot{\theta}_2^2\cos\theta_2 \\ -m_2 g\sin(\theta_1+\phi) - m_L r b\dot{\theta}_2^2 \sin(\theta_1-\theta_2) \\ m_L b g \sin(\theta_2+\phi) + m_L r b \dot{\theta}_1^2 \sin(\theta_1 - \theta_2) \end{bmatrix}
\end{aligned}$$

### B. Stability of Limit Cycle around Fixed Point

In this section, the derivation of Eq. (25) is explained [17]. When there is a small perturbation at $k$-th impact $\Delta\boldsymbol{x}^{(k)}$ from a fixed point $\boldsymbol{x}^*$, the discrete state variable vector $\boldsymbol{x}^{(k)}$ is expressed as follows.

$$\boldsymbol{x}^{(k)} = \boldsymbol{x}^* + \Delta\boldsymbol{x}^{(k)} \tag{21}$$

Similarly, the discrete state variable vector at ($k$+1)-th impact is represented as follows.

$$\boldsymbol{x}^{(k+1)} = \boldsymbol{x}^* + \Delta\boldsymbol{x}^{(k+1)} \tag{22}$$

When the change in state for each step is described as $\boldsymbol{x}^{(k+1)} = \boldsymbol{f}(\boldsymbol{x}^{(k)})$, the $(k+1)$-th state vector can be expressed using first-order Taylor series expansion as

$$\begin{aligned}
\boldsymbol{x}^{(k+1)} &= f(\boldsymbol{x}^* + \Delta\boldsymbol{x}^{(k)}) \\
&\approx f(\boldsymbol{x}^*) + \left.\frac{\partial f}{\partial \boldsymbol{x}}\right|_{\boldsymbol{x}=\boldsymbol{x}^*} \Delta\boldsymbol{x}^{(k)}
\end{aligned} \tag{23}$$

By the definition of a fixed point, $\boldsymbol{f}(\boldsymbol{x}^*) = \boldsymbol{x}^*$ holds, and thus the above equation becomes as follows.

$$\boldsymbol{x}^{(k+1)} \approx \boldsymbol{x}^* + \left.\frac{\partial f}{\partial \boldsymbol{x}}\right|_{\boldsymbol{x}=\boldsymbol{x}^*} \Delta\boldsymbol{x}^{(k)} \tag{24}$$

From Eqs. (22) and (24), the following equation can be derived:

$$\Delta\boldsymbol{x}^{(k+1)} \approx \boldsymbol{J}\Delta\boldsymbol{x}^{(k)}, \ \ \boldsymbol{J} := \left.\frac{\partial \boldsymbol{f}}{\partial \boldsymbol{x}}\right|_{\boldsymbol{x}=\boldsymbol{x}^*}. \tag{25}$$

## REFERENCES


[1] T. McGeer, "Passive dynamic walking," *The Int. J. Robotics Reserch*, Vol. 9, No. 2, pp. 62-82, 1990.

[2] A. Goswami, B. Thuilot and B. Espiau, "Compass-like biped robot part I: stability and bifurcation of passive gaits," *Research Report*, No. 2996, 1996.

[3] B. Thuilot, A. Goswami and B. Espiau, "Bifurcation and chaos in a simple passive bipedal gait," *Proc. of Int. Conf. on Robotics and Automation*, Vol. 1, pp. 792-798, 1997.

[4] A. Goswami, B. Thuilot and B. Espiau, "A study of the passive gait of a compass-like biped robot: Symmetry and chaos," *The Int. J. of Robotics Research*, Vol. 17, No. 12, pp. 1282-1301, 1998.

[5] M. J. Kurz and N. Stergiou, "Hip Actuations Can be Used to Control Bifurcations and Chaos in a Passive Dynamic Walking Model," *ASME J. of Biomech. Eng.*, Vol. 129, No. 2, pp. 216-222, 2007.

[6] T. T. Lee and J. H. Liao, "Trajectory planning and control of a 3-link biped robot," *Proc. IEEE Int. Conf. on Robotics and Automation*, Vol. 2, pp. 820-823, 1988.

[7] T. Narukawa, M. Takahashi and K. Yoshida, "Biped locomotion on level ground by Torso and swing-leg control based on passive-dynamic walking," *IEEE/RSJ Int. Conf. on Intelligent Robots and Systems*, pp. 4009-4014, 2005.

[8] P. X. M. La Hera, A. S. Shiriaev, L. B. Freidovich, U. Mettin and S. V. Gusev, "Stable walking gaits for a three-link planar biped robot with one actuator," *IEEE Trans. on Robotics*, Vol. 29, No. 3, pp. 589-601, 2013.

[9] S. Tzafestas, M. Raibert and C. Tzafestas, "Robust sliding-mode control applied to a 5-link biped robot," *J. of Inteligent and Robotic Systems*, Vol. 15, pp. 67-133, 1996.

[10] H. K. Lum, M. Zribi and Y. C. Soh, "Planning and control of a biped robot," *Int. J. of Engineering Science*, Vol. 37, No. 10, pp. 1319-1349, 1999.

[11] E. Borzova and Y. Hurmuzlu, "Passively walking five-link robot," *Automatica*, Vol. 40, No. 4, pp. 621-629, 2004.

[12] J. Kieffer and R. Bale, "Walking viability and gait synthesis for a novel class of dynamically-simple bipeds," *Informatica*, Vol. 17, No. 2, pp. 145-155, 1993.

[13] M. W. Spong, "An almost linear biped," *Proc. of IEEE Conf. on Decision and Control*, Vol. 5, pp. 4803-4808, 2000.

[14] F. Asano and C. Yan, "Low-speed limit cycle walking of planar X-shaped bipedal robot with special properties," *Int. Conf. on Advanced Robotics and Mechatronics*, pp. 43-48, 2023.

[15] F. Asano, T. Sedoguchi and C. Yan, "Generation of steady weel gait for planar X-shaped walker with Reaction wheel," *IEEE Int. Conf. on Robotics and Automation*, pp. 5766-5772, 2024.

[16] F. Asano, M. Komori, T. Sedoguchi and Y. Zheng, "Stable wheel gait generation for planar X-shaped walker with telescopic legs based on asymmetric impact posture," *IEEE/RSJ Int. Conf. on Intelligent Robots and Systems*, pp. 11117-11122, 2024.

[17] Y. Ikemata, A. Sano and H. Fujimoto, "A physical principle of gait generation and its stabilization derived from mechanism of fixed point," *Proc. of IEEE Int. Conf. on Robotics and Automation*, pp. 836-841, 2006.

[18] M. Garcia, A. Chatterjee, A. Ruina and M. Coleman, "The simplest walking model: stability, complexity, and scaling," *J. of Biomech. Eng.* pp. 281-288, 1998.